Strengthening Slender Reinforced Concrete Columns Using High-Modulus Bonded Longitudinal...

Article *in* Journal of Structural Engineering · April 2015

DOI: 10.1061/(ASCE)ST.1943-541X.0001066

CITATION
1

READS
35

2 authors:

Pedram Sadeghian
Dalhousie University
23 PUBLICATIONS **66** CITATIONS
SEE PROFILE

Amir Fam
Queen's University
177 PUBLICATIONS **1,804** CITATIONS
SEE PROFILE

STRENGTHENING OF SLENDER REINFORCED CONCRETE COLUMNS BY BUCKLING CONTROL USING HIGH-MODULUS BONDED LONGITUDINAL REINFORCEMENT

Pedram Sadeghian, M.ASCE [1] and Amir Fam, M.ASCE [2]

ABSTRACT

This paper introduces a model for strengthening slender reinforced concrete columns. The proposed technique aims at controlling second order lateral deflections using longitudinal high-modulus bonded reinforcement, thereby altering the loading path to intercept the axial load-moment (P-M) interaction curve at a higher axial capacity. With the availability of high- and ultra-high-modulus carbon fiber reinforced polymer (CFRP) plates, this approach should be quite efficient according to Euler's buckling rule, in which, column strength is stiffness-controlled. This approach is different from the classical transverse wrapping method for confinement; a technique that achieves strengthening by enlarging the (P-M) diagram in the compression-controlled region. The proposed model accounts for concrete nonlinearity in compression, cracking in tension, steel rebar plasticity, and certainly geometric nonlinearity, in addition to the possibility of premature CFRP debonding failure in tension and the lower CFRP strength in compression than tension. The model is validated against experimental results and used in a parametric study to assess the effects of slenderness ratio λ, axial load initial eccentricity ratio e_o/h, and CFRP reinforcement ratio ρ_f, and modulus E_f. It was shown that strength gain increases from 17 to 30% as λ increases from 20 to 120, when a very small ρ_f of 0.5% is used. A range of 0.1 to 1% for ρ_f results in a 4 to 41% strength gain, while a range of 100 to 500 GPa for E_f results in a 5 to 26% gain. As e_o/h increases from 0.05 to 0.6, the gain increases from 17 to 90%.

[1] Assistant Professor of Civil Engineering, Penn State Harrisburg, Middletown, PA, 17057; and Former Postdoctoral Fellow, Queen's University, Kingston, ON, K7L 3N6 Canada. E-mail: pedram@psu.edu

[2] Professor and Canada Research Chair in Innovative and Retrofitted Structures, Department of Civil Engineering, Queen's University, Kingston, ON, K7L 3N6 Canada. E-mail: fam@civil.queensu.ca

Keywords: slender column, reinforced concrete, buckling, CFRP, high-modulus, strengthening.

INTRODUCTION

In the past two decades fiber reinforced polymer (FRP) composites have emerged in structural engineering as a retrofitting material with superior characteristics for existing reinforced concrete (RC) structures. One of the most common and effective applications, and perhaps the most widely researched area to date, is RC column confinement using FRP wraps. It is now widely accepted that applying transverse unidirectional FRP thin sheets to short columns effectively provides significant lateral confinement of the concrete core, leading to considerable increase in the unconfined concrete compressive strength and ductility of the columns under concentric axial compressive loadings (Shahawy et al. 2000; Pessiki et al. 2001; Lam and Teng 2003; and Mandal et al. 2005). This system is much more effective for RC columns with circular cross section than rectangular sections. Also, transverse FRPs have been successfully examined for strengthening RC short columns under eccentric compressive loadings (Parvin and Wang 2001; Li and Hadi 2003; and Hadi 2007). It is well established that transverse FRP wraps can enlarge the axial load-bending moment (P-M) interaction resistance curves of RC sections in the compression-control region (i.e. under combined large axial loads and low bending moments), as shown in Fig. 1(a), by shifting the column strength from point A to A' (Saadatmanesh et al. 1995 and Bisby and Ranger 2010).

The effects of a combination of transverse and longitudinal FRP systems on RC columns have been studied by some researchers (Chaallal and Shahawy 2000; Fam et al. 2003; Sadeghian et al. 2010; and Quiertant and Clement 2011), but their main focus has been on short columns and the effect of FRPs on the P-M interaction resistance curves, not on the effects of slenderness and load path. Moreover, in some design guidelines such as ACI 440.2R (2008) there is a gap regarding slender RC columns strengthened with FRPs. Recently, some studies (Fitzwilliam and

Bisby 2010 and Jiang and Teng 2011) have been conducted on FRP strengthening of slender RC columns, but their target has been primarily enlarging the P-M interaction resistance curves and upgrading the columns through applying transverse FRPs to enhance confinement.

Hypothesis of the Proposed Model

It has been well established that longitudinal FRP strengthening systems such as longitudinal fabrics, bonded laminates, and near surface mounted (NSM) systems can only enhance the strength of RC columns under large bending moment and small axial load (i.e. by enlarging the P-M interaction curve in the tension-controlled region), as shown in Fig. 1(b). It has also been recognized that this longitudinal FRP system may have insignificant strengthening effect for columns under large axial load and small moment. This is due to the belief that longitudinal FRP may not be reliable in compression especially when its stiffness is low, as in the case of Glass-FRP (GFRP). This is true for a short column with a low-stiffness FRP reinforcement, where the shift of point A to A' in Fig. 1(b) is small, however, for slender RC columns the behavior is quite different and this problem has not been addressed before.

This paper presents a new model for slender RC columns strengthened by a longitudinal FRP system and subjected to large axial loads and small initial moments. The fundamental aspect of this model, and perhaps a key difference from other strengthening approaches, is that it seeks the desired strength gain of the column primarily by altering the loading path (from OB to OB' in Fig. 1(b)), such that it intercepts the P-M interaction curve at a higher point. The approach then - to a lesser extent - relies on enlarging the P-M resistance curve as in the traditional FRP-strengthening philosophy. The axial strength of slender columns in many cases is governed by stability failure in the form of global buckling before reaching material failure, according to Euler's rule, where the strength is directly a function of the cross-sectional stiffness

(*EI*). With the emergence of new generations of ultra-high modulus CFRP reinforcement (well in excess of 200 GPa), these materials are ideal for strengthening slender members against stability failure. The light weight, thin profile and ease of adhesive-bond installation of CFRP plates to concrete surface makes this concept much easier to apply and likely more cost effective compared to traditional concrete jacketing methods of columns, which also increase column size considerably. In fact, this concept was successfully demonstrated by Shaat and Fam (2009) for strengthening slender steel hollow rectangular section columns.

The proposed model accounts for material nonlinearity of concrete in compression, concrete cracking in tension, steel reinforcement plasticity, and of course geometric nonlinearity of the slender column in the form of second order deformations. The model also considers the possibility of premature CFRP debonding failure in tension as well as the lower CFRP crushing strength compared to tensile rupture. The model is validated against experimental results and used in a comprehensive parametric study to assess the effects of slenderness ratio, initial eccentricity of load, CFRP reinforcement ratio, and CFRP modulus.

ANALYTICAL MODELING

The objective of the model is to predict the loading path and ultimate load of slender RC columns strengthened with longitudinal high modulus CFRPs. As shown in Fig. 1(b), the loading paths (OB or OB') are nonlinear and their nonlinearity is function of slenderness ratio and flexural stiffness of the column. In general, the loading path could have ascending and descending branches, with a peak load which corresponds to buckling load (i.e. stability failure). For ordinary RC columns with moderate slenderness, the ascending branch intercepts the P-M interaction curve (i.e. material failure) before reaching the peak and descending. The intercept of P-M interaction curve may occur in the tension- or compression-control regions. For RC

columns with high slenderness ratio, the load path reaches the peak bucking load and the descending branch intercepts the P-M interaction curve at a lower load. It should be mentioned that the P-M interaction curve is only function of cross-section geometry and material properties but not a function of length or end conditions (i.e. slenderness). The latter, however, directly affects the loading path and its nonlinear shape due to second order deformations.

In order to plot the load path of a column, axially loaded at a given initial eccentricity e_o (Fig. 1(b)), an iterative analysis is required at any given load/displacement level to capture the second order deformation of the column. The initial bending moment Pe_o produces a lateral deformation δ_o, which increases the eccentricity at mid-height to ($e_o+\delta_o$). The new eccentricity creates an additional bending moment $P\delta_o$, which in turn generates an additional deflection, and this procedure continues until convergence is reached at a final lateral deflection δ and a final moment $P(e_o+\delta)$. This iterative procedure is then performed at different load/displacement levels to establish enough points for the entire load path to failure. The first step in this procedure is a 'moment-thrust-curvature' analysis carried out for the FRP-strengthened RC cross-section.

Section Analysis

Figure 2(a) shows a RC column with rectangular cross-section (width b × height h) and longitudinal steel reinforcements at the tension side with a total area A_s at an effective depth d, measured from the extreme concrete fiber in compression. Also, the steel reinforcement at mid-section has a total area A_{sm} at an effective depth d_m (can be $0.5h$), and at the compression side the total steel area is A'_s at an effective depth d'. The column is strengthened with longitudinal bonded FRP plates or NSM FRP bars/strips at the extreme fibers of both sides, including total areas of A_f and A'_f on the tension and compression sides, at effective depths d_f and d'_f, respectively. d'_f is a negative value for externally bonded FRP and positive for NSM FRP.

It is assumed that the strain profile is linear and FRP, steel and concrete are perfectly bonded without any slip, as shown in Fig. 2(b), until either material failure occurs or FRP premature debonding occurs, as discussed in the failure criteria section. Thus, strains at steel reinforcements (i.e. ε_s, ε_{sm}, and ε'_s) and at FRPs (i.e. ε_f and ε'_f) are proportional with the maximum concrete strain ε_c in compression and curvature ψ. The column is under compressive axial load P at eccentricity e (with respect to mid height $h/2$ of the concrete section) as shown in Fig. 2(c). Tensile concrete is neglected and neutral axis depth c is measured from the extreme concrete compression fiber. As there is no transverse FRP for confinement, compressive behavior of unconfined concrete can be adequately described by the Popovics model (Popovics 1973). As shown in Fig. 2, the compressive stress f_c at distance y from the neutral axis, corresponding to a strain ε_c, is given by:

$$f_c = \frac{f'_c\left(\varepsilon_c / \varepsilon'_c\right)r}{r-1+\left(\varepsilon_c / \varepsilon'_c\right)^r} \qquad (1)$$

where f'_c is unconfined concrete strength, ε'_c is corresponding strain, and $r=E_c/(E_c-E_{sec})$. The elastic modulus E_c, secant modulus E_{sec}, and ε'_c are determined as $E_c=4700\sqrt{f'_c}$ in MPa, $E_{sec}=f'_c/\varepsilon'_c$, and $\varepsilon'_c=1.7f'_c/E_c$; respectively. In order to develop the P-M interaction curve, the maximum useable strain ε_{cu} at the extreme compression fiber of unconfined concrete (i.e. at crushing) is assumed equal to 0.003 (ACI 318 (2011) and ACI 440-2R (2008)).

The behavior of steel reinforcements is assumed linear elastic-perfectly plastic with elastic modulus E_s, yielding stress f_y, and yielding strain ε_y. The behavior of FRPs is assumed linear elastic with elastic modulus E_f up to tensile rupture stress f_{ftu} (tensile rupture strain ε_{ftu}) and compressive crushing stress f_{fcu} (compressive crushing strain ε_{fcu}), which is likely lower than the tensile strength. Based on Fig. 2(b), strain ε_c at any concrete compression fiber is evaluated as

$\varepsilon_c=\psi.y$ and strain ε_{cm} at extreme concrete compression fiber (i.e. at $y=c$) is evaluated as $\varepsilon_{cm}=\psi.c$. Thus, the resultant force C_c corresponding to compressive concrete and its moment M_c at point A (Fig. 2(c)), at extreme concrete compression fiber, can be expressed as the following:

$$C_c = b\int_a^c f_c dy \tag{2}$$

$$M_c = b\int_a^c (c-y) f_c dy \tag{3}$$

where a is zero when neutral axis is inside the concrete section and is (c-h) when neutral axis is outside. For steel reinforcements, strain ε_s, ε_{sm}, and ε'_s are evaluated as $\varepsilon_s=\psi(d-c)$, $\varepsilon_{sm}=\psi(d_m-c)$, and $\varepsilon'_s=\psi(c-d')$, respectively. Thus, resultant forces T_s, T_{sm}, and C_s corresponding to tensile, mid-section, and compressive steel reinforcements can be expressed as the following:

$$T_s = \begin{cases} E_s\varepsilon_s, & -\varepsilon_y \le \varepsilon_s \le \varepsilon_y \\ f_y A_s, & \varepsilon_y \le \varepsilon_s \\ -f_y A_s, & \varepsilon_s \le -\varepsilon_y \end{cases} \tag{4}$$

$$T_{sm} = \begin{cases} E_s\varepsilon_{sm}, & -\varepsilon_y \le \varepsilon_{sm} \le \varepsilon_y \\ f_y A_{sm}, & \varepsilon_y \le \varepsilon_{sm} \\ -f_y A_{sm}, & \varepsilon_{sm} \le -\varepsilon_y \end{cases} \tag{5}$$

$$C_s = \begin{cases} E_s\varepsilon'_s, & -\varepsilon_y \le \varepsilon'_s \le \varepsilon_y \\ f_y A'_s, & \varepsilon_y \le \varepsilon'_s \\ -f_y A'_s, & \varepsilon'_s \le -\varepsilon_y \end{cases} \tag{6}$$

For FRPs, strain ε_f and ε'_f are evaluated as $\varepsilon_f=\psi(d_f-c)$ and $\varepsilon'_f=\psi(c+d'_f)$, respectively. Thus, resultant forces T_f and C_f corresponding to tensile and compressive FRPs can be expressed as the following:

$$T_f = E_f\varepsilon_f A_f \tag{7}$$

$$C_f = E_f\varepsilon'_f A'_f \tag{8}$$

To this end, the internal forces have been expressed in terms of two main parameters, namely; curvature ψ and neutral axis depth c. By applying static equilibrium conditions, considering internal and external forces (Fig. 2(c)), the following two equations are derived:

$$C_c + C_s + C_f - T_s - T_{sm} - T_f = P \tag{9}$$

$$M_c + C_s(d') - T_s(d) - T_{sm}(d_m) - T_f(d_f) - C_f(d'_f) = P(0.5h - e) \tag{10}$$

For a given eccentricity e and load P, Equations (9) and (10) are sufficient to obtain the two unknown parameters (curvature ψ and neutral axis depth c), using a conventional computer program. A characteristic P-M interaction diagram can then be established for the cross-section based on the failure criteria discussed in the following section. Also, the calculated curvatures will be used for the lateral deflection calculations of slender RC columns through an iterative analysis which is discussed later.

Failure Criteria

Material failure: The model accounts for material failure in the form of (a) concrete crushing at a 0.003 compressive strain ε_{cu}, (b) steel yielding in tension and/or compression at stress f_y, (c) FRP tensile rupture at strength f_{ftu}, or FRP compressive crushing at strength f_{fcu}.

FRP debonding failure: Based on ACI 440.2R (2008), a failure controlled by FRP debonding may occur away from where externally-bonded FRP terminates. To check for that intermediate crack-induced debonding failure, the tensile strain in FRP reinforcement should be checked at every step and compared to the effective strain at which debonding may occur, ε_{fd}, as follows:

$$\varepsilon_{fd} = 0.41\sqrt{\frac{f'_c}{nE_f t_f}} \tag{11}$$

where E_f and t_f are the elastic modulus and thickness of a single ply of the FRP laminate, n is the number of plies, and f'_c is compressive strength of concrete. If the debonding strain ε_{fd} is larger

than the ultimate rupture strain of the FRP laminate in tension, ε_{fu}, this means that the section is not vulnerable to debonding failure and that reaching FRP rupture is possible. The FRP debonding failure affects the resistance in the form of the P-M interaction curve in the tension-controlled region by reducing the capacity. Material failure occurs once the loading path intercepts the P-M envelope, while stability failure occurs if the loading path reaches a peak inside the P-M curve before it intercepts the envelope. The effect of premature debonding on P-M curves will be illustrated in detail in the parametric study section.

Analysis of Slender Columns for the Ascending Load Path

For a deformed slender column under eccentric compressive load *P*, the eccentricity *e* varies along the length from the initial eccentricity e_o. Distribution of eccentricity *e* is coupled with lateral deflection; therefore, an iterative analysis is necessary. Consider a RC column with length *L* under symmetric bending, as shown in Fig. 3 for one half of the column. Lateral deflection varies from zero at the end A to maximum at mid-height point M, thus the tangent of deformed shape at point M is parallel to the original axis of the column. Consider a general point X at a distance x from point A. The lateral deformation δ_X at point X is expressed as $\delta_X = x.\theta_A - t_{X/A}$, where θ_A is the slope at point A and $t_{X/A}$ is the horizontal distance between the extended tangent of point A and point X on the deformed column (Fig. 3). Using the moment-area method, the tangent slope at A, θ_A, and $t_{X/A}$ can be expressed as the following:

$$\theta_A = \int_0^{L/2} \psi(z)dz \tag{12}$$

$$t_{X/A} = \int_0^{x} \psi(z)(x-z)dz \tag{13}$$

Where $\Psi(z)$ is the curvature at a section at distance *z* from the top. Thus, lateral deflection δ_X at position *x* is expressed as:

$$\delta_X = x\int_0^{L/2}\psi(z)dz - \int_0^{x}\psi(z)(x-z)dz \qquad (14)$$

Numerical integration is then used to solve Equation (13). The column of length L is equally divided to n number of segments with segment length of $\Delta x=L/n$, as shown in Fig. 3. Thus, lateral deformation δ_i at position x_i (i.e. node number i with curvature ψ_i) can be expressed as the following:

$$\delta_i = x_i\left[\sum_{j=1}^{n/2}\left(\frac{\psi_j+\psi_{j-1}}{2}\right)\Delta x\right] - \left[\sum_{j=1}^{i}\left(\frac{\psi_j+\psi_{j-1}}{2}\right)\left(x_i - x_j + \frac{\Delta x}{2}\right)\Delta x\right] \qquad (15)$$

For a given cross-section with a known end eccentricity e_o, apply a known axial load P and the goal is to compute the total lateral deflection at mid-height ($e_o+\delta_M$). The procedure starts as follows: Calculate the curvature due to the load P and moment $P.e_o$ using the procedure described earlier. In the first iteration, curvature is constant at all nodes along the length under the constant moment $P.e_o$ because the column is not laterally deflected yet. Using Equation (15), deformation at each node can be calculated. In the second iteration, eccentricity at each node is equal to the initial eccentricity e_o plus the corresponding deformation δ_i. Thus at each node a new section analysis (as presented in the previous section) with new eccentricity ($e_o+\delta_i$) can be performed to calculate a new curvature ψ_i under known axial load P and moment $P(e_o+\delta_i)$. Using Equation (15), new deformations can be calculated for the third iteration. This iterative analysis is continued until convergence occurs for the maximum deflection at mid-height, δ_M. Convergence has been defined here as a deformation increment equal to or less than 0.01 mm. At the end of this iterative analysis, one point on the load path has been established with the coordinates [$P(e_o+\delta_M)$, P]. The process is then repeated for a higher axial load $P+\Delta P$ (i.e. a load control approach) and a new point is obtained on the ascending load path, and so on. The process continues until the load path intercepts the (P-M) interaction curve (for moderate slenderness) or until it reaches a peak before it intercepts the curve (for large slenderness).

In columns with large slenderness, a typical load path goes through a descending branch once the peak load is reached. To capture the peak load, load steps ΔP should be refined to obtain adequate number of points and capture the peak load which reflects the maximum column capacity and indicates a stability failure, not a material failure. The technique described so far can only capture the ascending branch because it is load-controlled. The next section presents a method to capture the descending load path, which continues until material failure eventually occurs when it intercepts the (P-M) interaction curve at a lower load. For most conventional slender RC columns, material failure usually governs but for certain conditions of slender RC columns, buckling failure may govern, where yielding of the tensile steel reinforcements can suddenly reduce stiffness of the column and triggers the buckling failure. In these cases, after a sharp-shaped peak, a short descending branch appears.

Analysis of Slender Columns for the Descending Load Path

The descending branch of the load path could be captured using a displacement-control approach. The analysis would be similar to that of the ascending branch, except that the load is calculated for a given lateral deflection. Given that the primary purpose of the model presented in this paper is to capture the peak load of the column, which is already accomplished in the previous section, the rigorous and time–consuming incremental displacement-control analysis of the post buckling behavior was deemed unnecessary. Instead, a simplified closed-form analysis is proposed by assuming a sign-curve deflected shape for the pinned RC column. This assumption of a sign-shape was suggested by Lloyd and Rangan (1996) and Claeson and Gylltoft (1998) and verified by Sadeghian et al. (2010). In the proposed simplified analysis, and for a given mid-height deflection δ_M, the unknowns are the load P; the curvature ψ_M and the neutral axis depth c_M. Thus, the two equilibrium equations of axial force and moment (Eqs. 9 and 10) at the mid-height section are not enough. An additional equation is developed based on the sign-

shape distribution of deflection. The distribution of curvature $\psi(x)$ along the length of the pinned column is assumed analogous to the sign-shape distribution of lateral deflection as follows:

$$\psi(x) = (\psi_M - \psi_o)\sin\frac{\pi x}{L} + \psi_o \tag{16}$$

where ψ_o is curvature at the support (at $x = 0$) and ψ_M is curvature at mid-height (at $x = L/2$). Using the moment-area method, deflection at mid-height δ_M is derived as follows:

$$\delta_M = (\psi_M - \psi_o)\int_0^{L/2} x\sin\frac{\pi x}{L}dx + \psi_o\frac{L^2}{8} \tag{17}$$

Equation 17 is a third equitation but it involves a fourth unknown, ψ_o. By adding two more equilibrium equations (Eqs. 9 and 10) being applied at the support section, a fifth unknown is also added, which is the neutral axis depth at the support c_o. For a given mid-height deflection δ_M, we now have five equations to solve for the following five unknowns: P, ψ_M, c_M, ψ_o, and c_o, of which, the primary unknown is P, which is then plotted against δ_M to establish the descending branch of the load path until it intercepts the (P-M) interaction diagram.

When applying this simplified method at the point of the peak load the load path, it results in a peak load that is smaller by 2 to 5% than that established at the end of the ascending curve using the rigorous iterative analysis. This is attributed to the simplified sign-shape assumption of the deflected column. In order to correct for this small discrepancy, the computed descending curve is shifted upward by this small percentage to provide a continuous curve for the entire loading path.

VERIFICATION

The proposed model is verified using experimental results from slender column tests. The first study was performed by Kim and Yank (1995) on conventional slender RC columns, where tests were carried out on 80×80 mm square tied columns of three slenderness ratios (λ) of 10, 60, and

100. Three different concrete strengths of 26, 64, and 86 MPa were used. Also, two different longitudinal steel reinforcement ratios of 1.98 and 3.95% were used. Hinged boundary conditions were used at both ends and the end loads were applied at 24 mm eccentricities at both ends, in the same direction. Figure 4 shows the predicted interaction diagrams of the 26 MPa concrete strength columns with the two different longitudinal steel reinforcement ratios. Also shown in Fig. 4 are the experimental and predicted load paths for different slenderness ratios, where the continuous line is the analytical load path. The figure shows good agreement between the analytical and experimental load paths. It is also shown that the loading path becomes more nonlinear, due to the increased second order effects, as slenderness ratio increases. Figure 4(b) shows that for λ=100, the load path reaches a peak load, followed by a very small descending branch just before intercepting the interaction curve. Figure 4(c) shows the axial load-lateral deflection curves, which also show good agreement between the model and experiment data for both ascending and descending branches.

The second study was performed by Shaat and Fam (2009) on slender steel columns strengthened with longitudinal CFRPs. The loading was applied concentrically on 44×44×3.2 mm hollow structural section (HSS) slender columns. Two layers of unidirectional pultruded CFRP plates, namely, 25x1.4 mm and 16x1.4 mm were adhesively bonded to the two opposite faces of the column, as shown in Fig. 5. The average tensile strength and elastic modulus of CFRP were 1475 MPa and 313 GPa, respectively. To be able to apply the RC model for this compact steel section, the RC cross-section geometry shown in Fig. 29(a) was manipulated such that the two flanges of the HSS section were entered as the extreme tensile and compressive reinforcement, while the two HSS webs were lump summed as the mid-section reinforcement. The concrete strength and modulus were entered as very low values close to zero. Figure 5

shows the axial load-lateral deflection curves of three identical specimens with slenderness ratio of 93, along with the predicted curve. The figure shows reasonable agreement between the analytical and experimental curves. Both curves show that overall buckling was the primary failure mode, followed by CFRP plate crushing at the inner face at about 15 mm lateral deflection. After CFRP crushing, the column continues with CFRP at one side only (i.e. the outer side), which the model is capable to predict. This behavior is discussed later in detail in the parametric study section.

The third experimental work was performed by Gajdosova and Bilcik (2013) on slender RC columns strengthened with longitudinal NSM CFRPs. To the authors' knowledge, this is the only available experimental study on slender RC columns strengthened with longitudinal FRPs. Full-scale slender rectangular RC columns were strengthened either with longitudinal NSM CFRP strips, transverse CFRP wraps, or a combination of both schemes. As shown in Fig. 6, the columns were 4.1 m long with 210×150 mm cross-sections. Longitudinal reinforcement of the columns consisted of 8 steel bars of 10 mm diameter and 6 mm stirrups spaced at 150 mm, with a 30 mm (reduced spacing) near both ends. For the two similar columns (Test 1 and Test 2) longitudinally-reinforced with NSM CFRP, three 3×15 mm longitudinal grooves were cut on each long-side of the column, cleaned and filled with epoxy adhesive and then 1.4×10 mm CFRP strips were inserted. The columns were hinge-supported at both ends, and axially loaded to failure with equal end eccentricities of 40 mm. Figure 6 shows the predicted interaction curve along with the experimental and predicted load paths. Reasonable agreement can be observed between the model and experimental load paths. The agreement is better with Test 1. The slight difference between Tests 1 and 2 experimental load paths may be attributed to slight friction at the hinge supports, but certainly within the expected range of experimental variation.

PARAMETRIC ANALYSIS

In this section, the analytical model is used in a parametric study to investigate the effects of key parameters on behavior of slender RC columns strengthened with longitudinal FRP reinforcement, including slenderness ratio ($\lambda=kL/r$); initial eccentricity ratio (e_o/h); FRP reinforcement ratio (ρ_f); and FRP modulus (E_f). When each parameter is being investigated, other parameters are kept constant and the default values are λ=60, e_o/h=0.1, ρ_f=0.5%, and E_f=400 GPa. The rest of parameters, namely f_{fu}=1500 MPa, f'_c=40 MPa, b=h=400 mm, f_y=400 MPa, E_s=200 GPa, and ρ_s=*2%* are kept constant. For some cases FRP debonding failure criterion governed. For example, for the default case, the effective debonding strain ε_{fd} calculated using Equation 11 was 0.00346, which is lower than the rupture strain ε_{fu} of 0.00375. This affects the tension-controlled region of the P-M curves, as shown in Figs. 7(a), 9, 11 and 13. In these figures, the dotted-parts of P-M diagrams of strengthened columns are based on FRP rupture, while the solid parts in tension-controlled regions are based on FRP debonding. It should be noted that FRP longitudinal strength (f_{ftu}) in compression is typically lower than in tension. As such, the relative strength has been included in the parametric study.

Effect of Slenderness Ratio

The range of slenderness ratios (λ) studied was 40 to 120. This range was selected to cover a wide yet practical range of possible slender columns encountered in practice from short to very slender. Figure 7(a) shows the P-M interaction curves of both control and strengthened columns using ρ_f of 0.5%, developed based on section analysis, using Equations 9 and 10. For FRP-strengthened sections, failure criterion for the compression-controlled region of the interaction curve was either concrete or FRP crushing, whichever occurred first, whereas failure criterion for the tension-controlled region was FRP rupture in tension, after yielding of steel. The load paths

are shown in Fig. 7(a) for each slenderness ratio, for both the control and strengthened counterparts. Figure 7(b) shows the load-lateral deflection responses of all cases. Figure 8 summarizes the results by showing variation of maximum axial load and percentage increase in maximum axial load with λ for both ρ_f of 0.5% (Fig. 8(a)) and ρ_f of 1% (Fig. 7(b)). Figure 8 clearly shows that as λ increased from 20 to 120, the percentage increase in axial load capacity increased from 17 to 30% for a 0.5% ρ_f and from 33 to 59% for the 1% ρ_f. The physical meaning of this observation is that bonding larger amount of longitudinal FRP to the surface of slender RC columns results in larger gains in axial capacity, with this gain becoming even larger as slenderness ratio increases. Also, Fig. 7(a) shows that for very slender columns (e.g. λ=80 to 120), the load paths reach a peak load signifying global buckling, then follows a descending branch that intercepts the interaction curve when material failure occurs at lower loads. Also, the load-lateral deflection responses of very slender columns have a rather extended post-peak plateau (Fig. 7(b)). It is noted that sudden loss of stiffness can occur due to steel yielding, FRP rupture, FRP crushing, or FRP debonding, while gradual loss of stiffness occurs as concrete strain increases, due to its non-liners stress-strain curve.

Effect of Initial Eccentricity Ratio

The initial eccentricity ratio (e_o/h) ranged from 0.05 to 0.6. Figure 9 shows the P-M interaction curves of the control and strengthened sections. The load paths for a column with λ=60 are presented in the figure for both control and strengthened cases. The dotted straight lines represent the corresponding short column path for each case. Figure 10 summarizes results by showing variation of maximum load and its percentage increase with (e_o/h). As (e_o/h) increases from 0.05 to 0.6, the percentage increase in load increases from 17 to 90%. As shown in Fig. 9, for (e_o/h) of 0.2 to 0.6, CFRP strengthening not only increased axial load but also changed the

failure mode from buckling of control column (load path with a peak and descending branch) to material failure of strengthened column (ascending load path intercepts P-M diagram). This is attributed to a fundamental change in the loading path by reducing second-order effects and not just enhancing the P-M resistance curve as typically happens in lateral confinement.

Effect of FRP Reinforcement Ratio

The FRP reinforcement ratio (ρ_f) is defined as the ratio of total area of longitudinal FRP reinforcements ($A_f + A'_f$) to gross area of concrete section (b×h). The range of ρ_f studied was zero to 1%. Figures11 (a) and (b) show the interaction curves and load paths for all cases of ρ_f, for λ equals 60 and 100, respectively. As ρ_f increases, the interaction diagram increases in size and also the load path changes. Figure 12 summarizes the results by showing the variation of percentage increase in axial load with ρ_f. As ρ_f increased from 0.1 to 1%, the percentage increase of axial load increased from 4 to 41%, for λ = 60 and from 5 to 55% for λ = 100, respectively. It is also worth noting that for λ = 60, the ρ_f of 0.7 and 1% changed failure mode from buckling to material failure, whereas for λ = 100, buckling failure always occurred (Fig. 11).

Effect of FRP Modulus

The range of FRP modulus (E_f) studied was 100 to 500 GPa. FRP strength in both tension and compression were assumed constant for the whole range of E_f (f_{fu}=1500 MPa). Figure 13 shows the interaction diagrams and load paths for different values of E_f. Figure 14 summarizes the results by showing the variations of percentage increase in axial load with E_f. As E_f increases from 100 to 500 GPa, the percentage increase in load increased from 5 to 26%. It is also noted that the higher the E_f, the less chance of buckling failure. For example, at E_f of 500 GPa, buckling failure was prevented and material failure governed the peak load.

Effect of FRP Lower Crushing Strength than Tensile Rupture

FRPs typically have compressive strengths (f_{fcu}) lower than their tensile strengths (f_{ftu}). The ratio α is introduced to define this ratio and was studied for the range of 0 to 1 (Figure 15(a)). FRP strength in tension is assumed constant at the default value for the whole range of α (f_{ftu}=1500 MPa). Figure 15(b) shows the interaction diagrams and load paths for different values of α. The FRP crushing was studied for the slenderness ratios 70 and 100. Line OA in Fig. 15(a) represents a typical load path of a FRP-strengthened RC column with the assumption of no FRP crushing until the loading path intercepts the P-M interaction curve at Point A. If the inner layer of FRP crushes, the load path changes at point B and the load drops to point B' on a new loading path OA' representing a column with FRP on the outer face only, until load path (OBB'A') intercepts the P-M curve at Point A'. Point B may be located before peak load (i.e. FRP crushing before overall buckling) or could be after peak load (i.e. overall buckling occurs before FRP crushing). In the latter scenario, the load capacity of the columns is not affected by FRP crushing.

The crushing of the inner FRP (i.e. location of point B) depends on compressive strength of the FRP. In Fig. 15(b), for λ=70 and α larger than 0.7, overall buckling occurs before FRP crushing. In this case, for α larger than 0.8, FRP crushing occurs beyond the interaction curve (i.e. FRP crushing strain is larger than concrete crushing strain of 0.003). For λ=100, α larger than 0.4 results in FRP crushing after overall buckling (i.e. past the peak). At λ=100, for α larger than 0.8, concrete crushing occurs before FRP crushing as in the case of λ=70.

CONCLUSIONS

In this paper an analytical model was developed to predict the behavior and strength of slender reinforced concrete (RC) columns strengthened with longitudinal high modulus bonded fiber

reinforced polymer (FRP) reinforcements. The key feature of the proposed method and the model is that it achieves strengthening primarily by altering the load path of the column, through controlling second order deflections, such that it intercepts the P-M interaction curve at a higher load. This is different from traditional strengthening approaches of RC columns, which aim primarily to enlarging the P-M interaction curve, rather than altering the loading path. The model accounts for material and geometric nonlinearity as well as concrete cracking. It is capable of capturing both the ascending and descending branches of the non-linear load paths when stability failure precedes material failure, in addition to cases where material failure precedes stability failure. After verification using experimental results, a comprehensive parametric study was conducted to examine several key column parameters. The following conclusions are drawn:

1. Efficiency of the strengthening technique increases as column slenderness ratio λ increases. As λ increased from 20 to 120, the percentage increase in axial load increased from 17 to 30% for a 0.5% CFRP reinforcement ratio ρ_f and from 33 to 59% for a 1% ρ_f.
2. As the initial load eccentricity ratio (e_o/h) increases, the efficiency of the strengthening technique increases significantly. When (e_o/h) increased from 0.05 to 0.6, the percentage increase in axial load increased from 17 to 90%.
3. Increasing CFRP longitudinal reinforcement ratio ρ_f increases the size of interaction diagram and alters the load path. As ρ_f increased from 0.1 to 1%, the percentage increase of axial load increased from 4 to 41%, for λ = 60 and from 5 to 55% for λ = 100.
4. The effectiveness of CFRP strengthening system increases as its modulus E_f increases. As E_f increased from 100 to 500 GPa, the percentage increase in load increased from 5 to 26%.
5. The longitudinal CFRP strengthening system not only increases axial strength but can also change failure mode. For example; for λ = 60, it changed failure mode from buckling of

control column to material failure of strengthened column in the following cases: when (e_o/h) was in the range of 0.2 to 0.6, when ρ_f was between 0.7 and 1%, and when E_f was 500 GPa.

ACKNOWLEDGEMENTS

The authors wish to acknowledge the financial support provided by the Ministry of Economic Development and Innovation of Ontario and Queen's University, through the Postdoctoral Fellowship provided to the first author and the Early Researcher Award and the Chancellor's Research Award provided to the second author.

NOTATION

A_f = area of typical tension FRP reinforcements;

A'_f = area of typical compression FRP reinforcements;

A_s = area of typical tension steel reinforcements;

A'_s = area of typical compression steel reinforcements;

A_{sm} = area of mid-section steel reinforcements;

b = width of rectangular cross section;

C_c = resultant force of compressive concrete;

C_f = resultant force of typical compression FRP reinforcements;

C_s = resultant force of typical compression steel reinforcements;

c = neutral axis depth

d = depth of typical tension steel reinforcements;

d' = depth of typical compression steel reinforcements;

d_m = depth of typical tension steel reinforcements;

d_f = depth of typical tension FRP reinforcements;

d'_f = depth of typical compression FRP reinforcements;

E_c = concrete elastic modulus;

E_f = FRP elastic modulus;

E_s = steel elastic modulus;

E_{sec} = concrete secant modulus;

e = axial load eccentricity;

e_o = initial axial load eccentricity;

f_c = stress of compressive concrete;

f'_c = unconfined concrete strength in compression;

f_{fu} = FRP strength when strength in tension and compression is the same;

f_{ftu} = FRP strength in tension;

f_{fcu} = FRP strength in compression;

f_{sy} = steel yielding strain;

h = height of rectangular cross section;

i = node number;

l = length of column;

M = bending moment;

M_c = resultant moment of compressive concrete;

n = number of column segments;

P = axial load;

r = gyration radius;

T_s = resultant force of typical tension steel reinforcements;

T_{sm} = resultant force of mid-section steel reinforcements;

T_f = resultant force of typical tension FRP reinforcements;

t = vertical deviation of tangent;

x = position along length of column;

y = position along height of cross section;

α = ratio of FRP compressive strength over tensile strength;

δ = lateral deformation;

δ_o = lateral deformation at the end of first iteration;

ε_c = strain of compression concrete;

ε'_c = strain of concrete at f'_c

ε_{cm} = maximum strain of compression concrete;

ε_{cu} = ultimate strain of compression concrete;

ε_f = strain of typical tension FRP reinforcements;

ε'_f = strain of typical compression FRP reinforcements;

ε_{fu} = FRP ultimate strain when strength in tension and compression is the same;

ε_{ftu} = FRP ultimate strain in tension;

ε_{fcu} = FRP ultimate strain in compression;

ε_m = strain of mid-section steel reinforcements;

ε_s = strain of typical tension steel reinforcements;

ε'_s = strain of typical compression steel reinforcements;

ε_y = steel yielding strain;

θ = slop of deformed shape column;

λ = slenderness ratios;

ρ_f = FRP reinforcement ratio;

ρ_s = steel reinforcement ratio; and

ψ = curvature.

REFERENCES

Shahawy, M., Mirmiran, A., and Beitelman, A. (2000). "Test and modeling of carbon-wrapped concrete columns." *Composites Part B: Engineering*, 31(6-7), 471–480.

Pessiki, S., Harries, K. A., Kestner, J., Sause, R., and Ricles, J. M. (2001). "The axial behavior of concrete confined with fiber reinforced composite jackets." *Journal of Composites for Construction*, 5(4), 237–245.

Lam, L., and Teng, J. G. (2003). "Design-oriented stress-strain model for FRP-confined concrete." *Construction and Building Materials*, 17(6-7), 471–489.

Mandal, S., Hoskin, A., and Fam, A. (2005). "Influence of concrete strength on confinement effectiveness of fiber-reinforced polymer circular jackets." *ACI Structural Journal*, 102(3), 383–392.

Parvin, A., and Wang, W. (2001). "Behaviour of FRP jacketed concrete columns under eccentric loading." *Journal of Composites for Construction*, 5(3), 146–152.

Li, J., and Hadi, M. N. S. (2003). "Behaviour of externally confined high strength concrete columns under eccentric loading." *Composite Structure*, 62(2), 145–153.

Hadi, M. N. S. (2007). "Behaviour of FRP strengthened concrete columns under eccentric compression loading." *Composite Structure*, 77(1), 92–96.

Saadatmanesh, H., Ehsani, M. R., and Li, M. W. (1994). "Strength and ductility of concrete columns externally reinforced with fiber composite straps." *ACI Structural Journal*, 91(4), 434–447.

Bisby, L., and Ranger, M. (2010). "Axial–flexural interaction in circular FRP-confined reinforced concrete columns." *Construction and Building Materials*, 24(9).1672–1681.

Chaallal, O., and Shahawy, M. (2000). "Performance of fiber-reinforced polymer-wrapped reinforced concrete column under combined axial-flexural loading." *ACI Structural Journal*, 97(4), 659–688.

Fam, A., Flisak, B., and Rizkalla, S. (2003). "Experimental and analytical modeling of concrete-filled fiber-reinforced polymer tubes subjected to combined bending and axial loads." *ACI Structural Journal*, 100(4), 1–11.

Sadeghian, P., Rahai A. R., and Ehsani, M. R. (2010). "Experimental study of rectangular RC columns strengthened with CFRP composites under eccentric loading." *Journal of Composites for Construction*, 14(4), 443–450.

Quiertant, M., and Clement, J. L. (2011). "Behavior of RC columns strengthened with different CFRP systems under eccentric loading." *Construction and Building Materials*, 25(2), 452–460

Fitzwilliam, J., and Bisby L. A. (2010). "Slenderness effects on circular CFRP confined reinforced concrete columns." *Journal of Composites for Construction*, 14(3), 280–288.

Jiang, T., and Teng, J. G. (2011). "Theoretical model for slender FRP-confined circular RC columns." *Construction and Building Materials*, doi:10.1016/j.conbuildmat.2010.11.109 (in Press).

Shaat, A., and Fam, A. (2009). "Slender steel columns strengthened using high-modulus CFRP plates for buckling control." *Journal of Composites for Construction*, 13(1), 2–12.

ACI 440.2R (2008). "Guide for the design and construction of externally bonded FRP systems for strengthening concrete structures." American Concrete Institute, Farmington, MI.

Popovics, S. (1973). "A numerical approach to the complete stress-strain curve of concrete." *Cement and Concrete Research*, 3(5), 583–599.

ACI 318 (2011). “Building code requirements for structural concrete.” American Concrete Institute, Farmington, MI.

Lloyd, N. A., and Rangan, B. V. (1996). “Studies on high-strength concrete columns under eccentric compression.” *ACI Structural Journal*, 93(6), 631–638.

Claeson, C., and Gylltoft, K. (1998). “Slender high-strength concrete columns subjected to eccentric loading.” *Journal of Structural Engineering*, 124(3), 233–240.

Kim, J. K., and Yang, J. K. (1995). “Buckling behaviour of slender high-strength concrete columns.” Engineering Structures, 17(1), 39-51.

Gajdosova, K., and Bilcik, J. (2013). “Full-Scale Testing of CFRP-Strengthened Slender Reinforced Concrete Columns.” Journal of Composites for Construction, 17(2), 239–248.

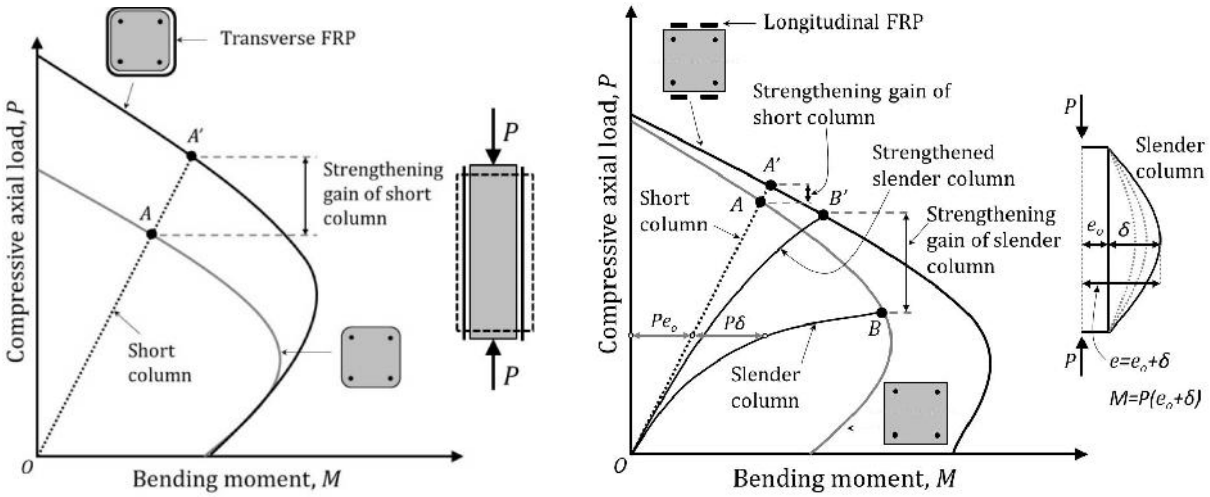

(a) Short column – by confinement **(b) Slender column – by controlling global buckling**

Fig. 1 Hypothesis of column strengthening using FRP retrofit systems

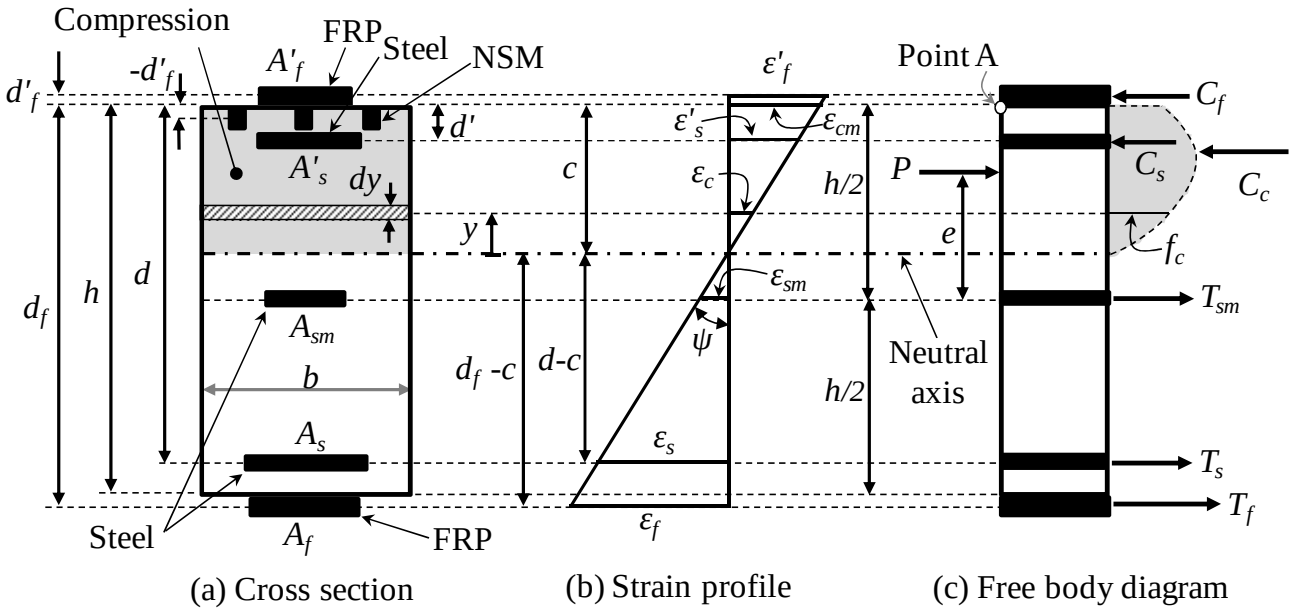

Fig. 2 Cross sectional analysis of a longitudinal-FRP-strengthened RC column with externally bonded FRP or NSM FRP

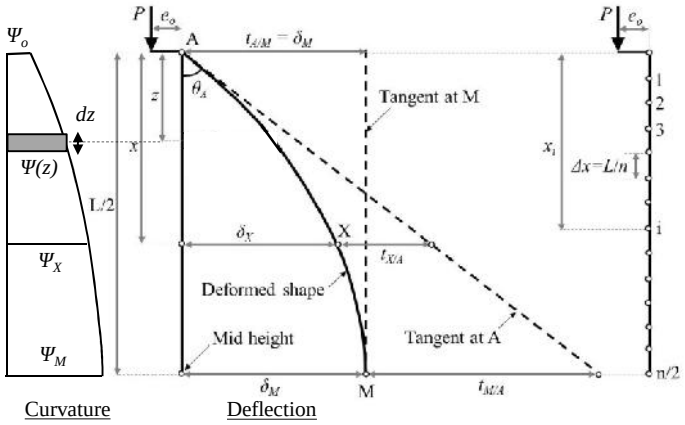

Fig. 3 Lateral deformation analysis of half-length of column

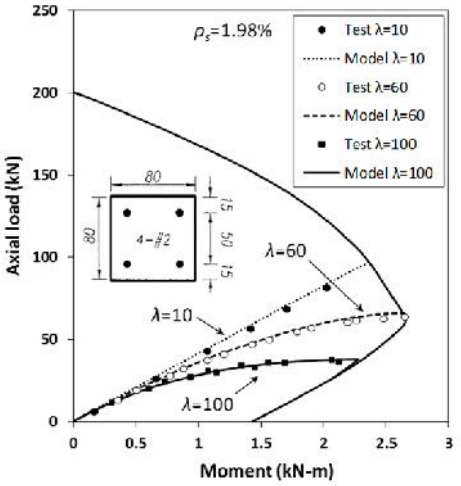

(a) 1.98% steel reinforcement ratio

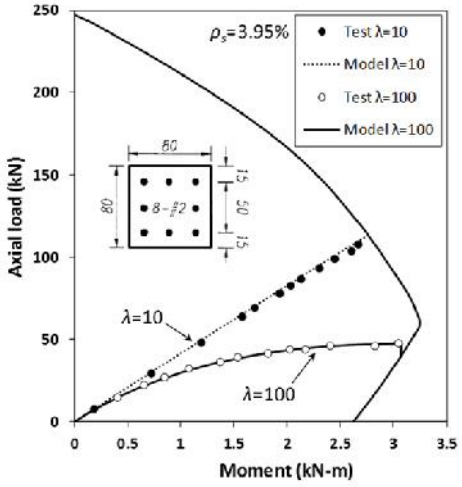

(b) 3.95% steel reinforcement ratio

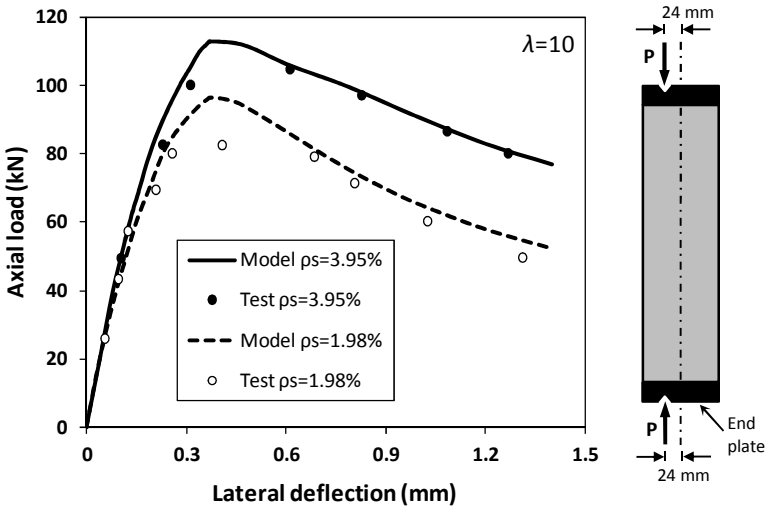

(c) Axial load – lateral deflection

Fig. 4 Model verification with experimental data of conventional RC columns of various slenderness ratios (Kim and Yank, 1995, dimensions in mm)

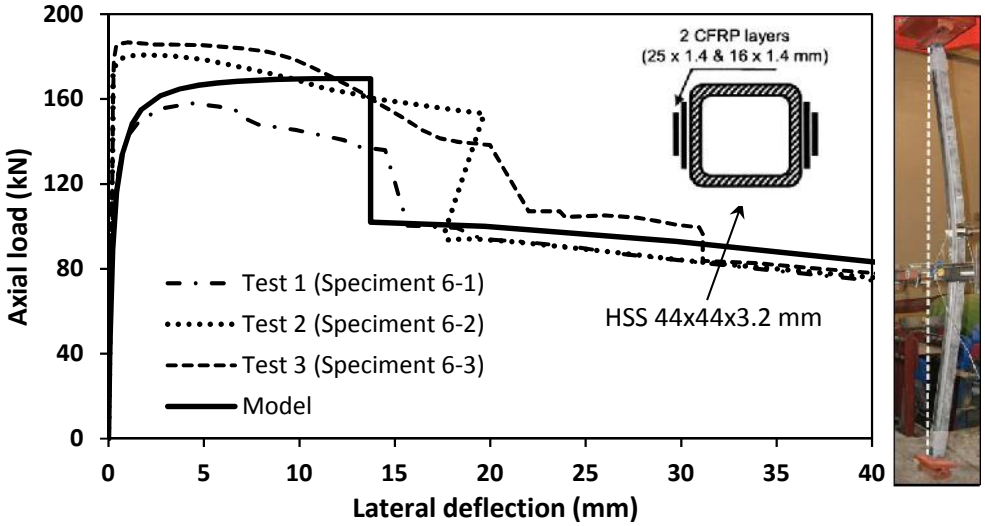

Fig. 5 Model verification with experimental data of slender steel columns strengthened with longitudinal CFRPs (reproduced from Shaat and Fam, 2009)

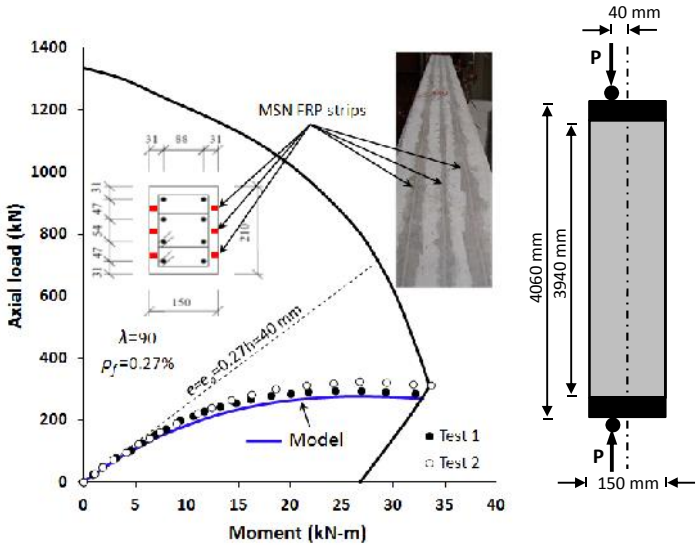

Fig. 6 Model verification with experimental data of slender RC columns strengthened with longitudinal NSM CFRPs (Gajdosova and Bilcik, 2013, dimensions in mm)

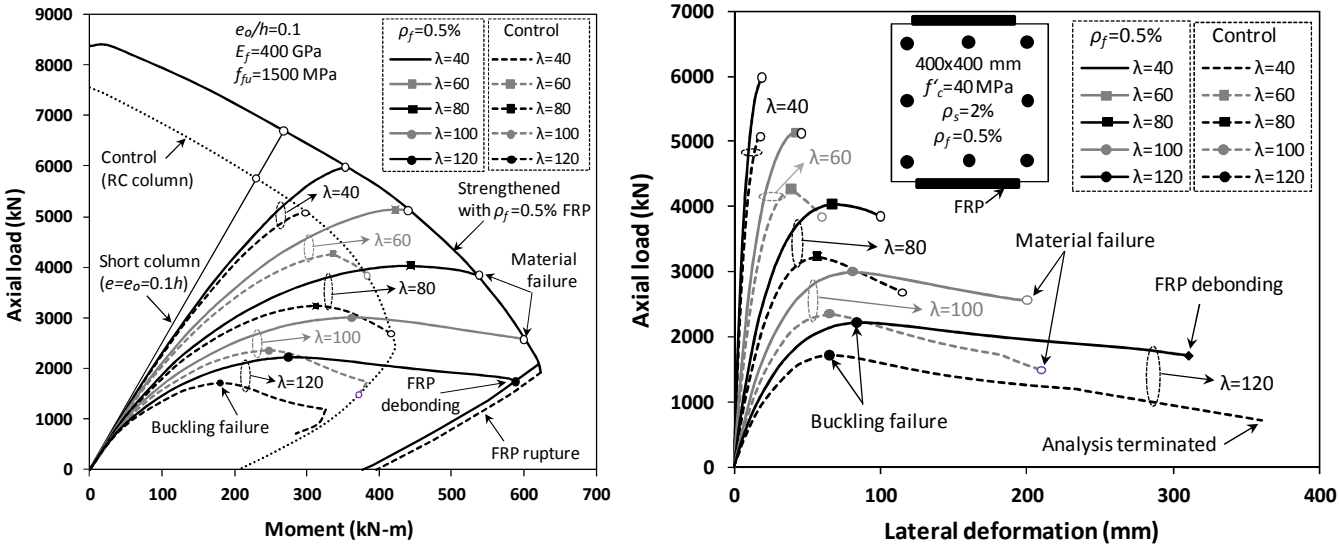

(a) Axial load-bending moment paths

(b) axial-load lateral deflection responses

Fig. 7 Performance of RC columns of various slenderness ratios

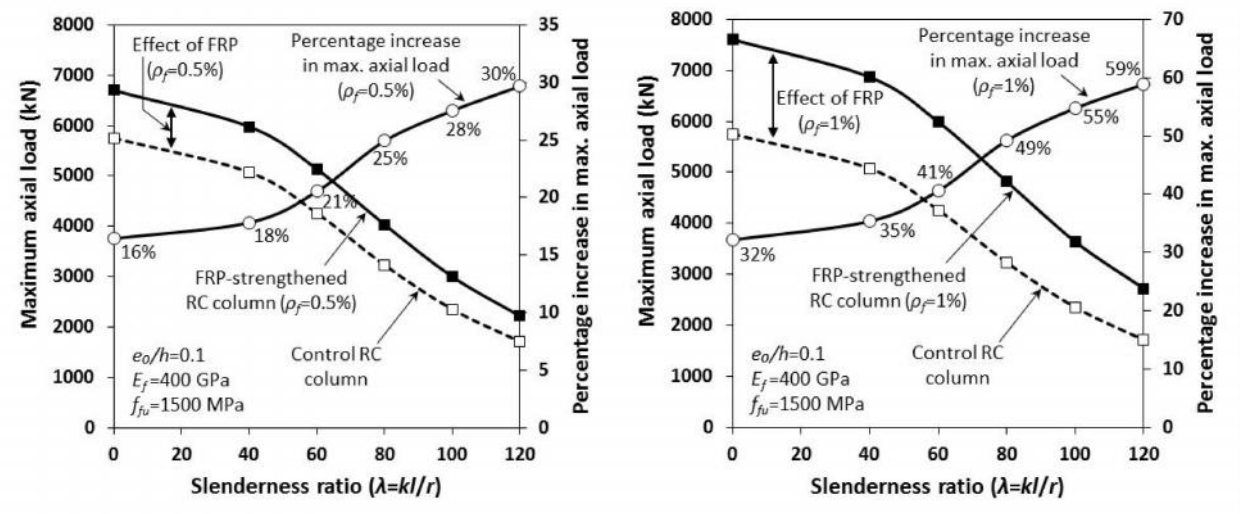

(a) 0.5% CFRP reinforcement ratio **(b) 1.0% CFRP reinforcement ratio**

Fig. 8 Variation of strength gain due to CFRP retrofitting with slenderness ratio of column

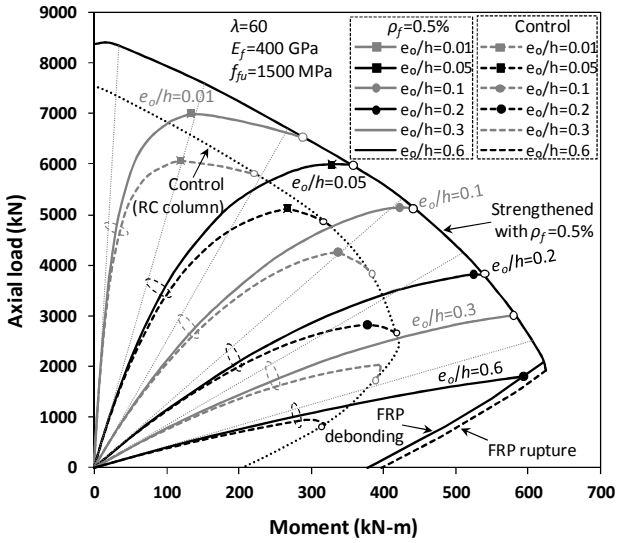

Fig. 9 Performance of RC columns of various initial eccentricities

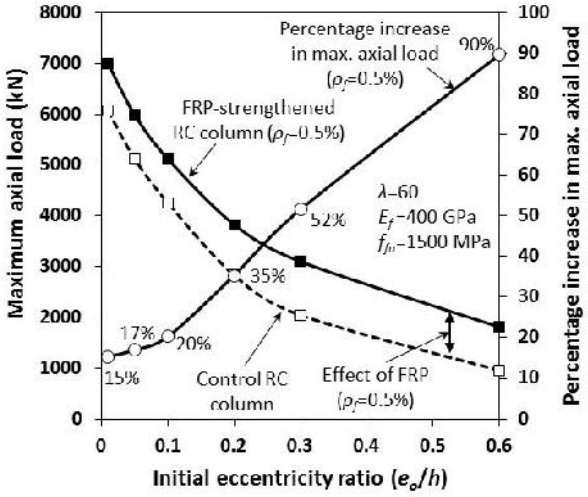

Fig. 10 Variation of strength gain due to CFRP retrofitting with initial eccentricity ratio of column

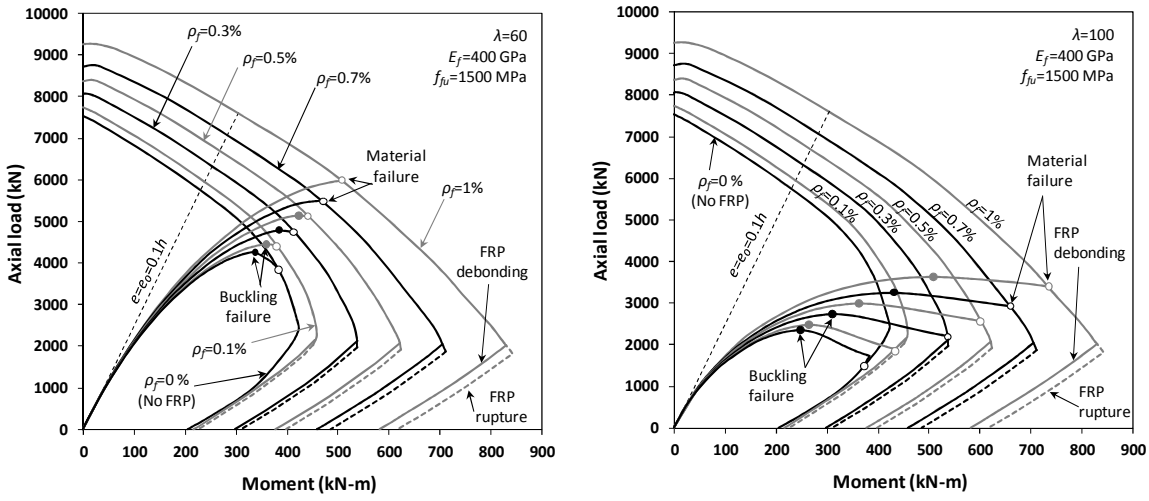

(a) Slenderness ratio of 60 **(b) Slenderness ratio of 100**

Fig. 11 Performance of RC columns of various CFRP reinforcement ratios

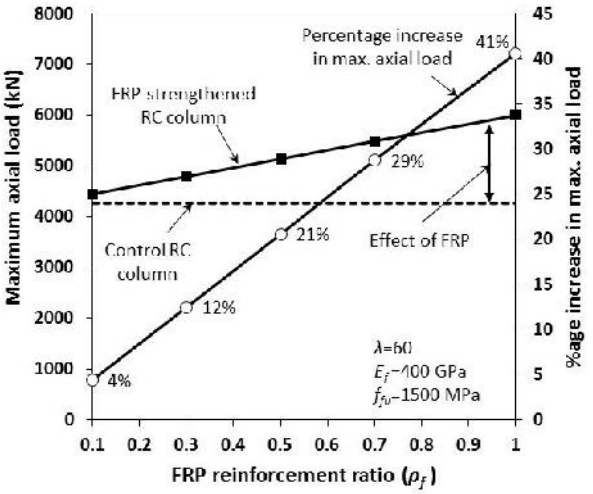

Fig. 12 Variation of strength gain due to CFRP retrofitting with CFRP reinforcement ratio

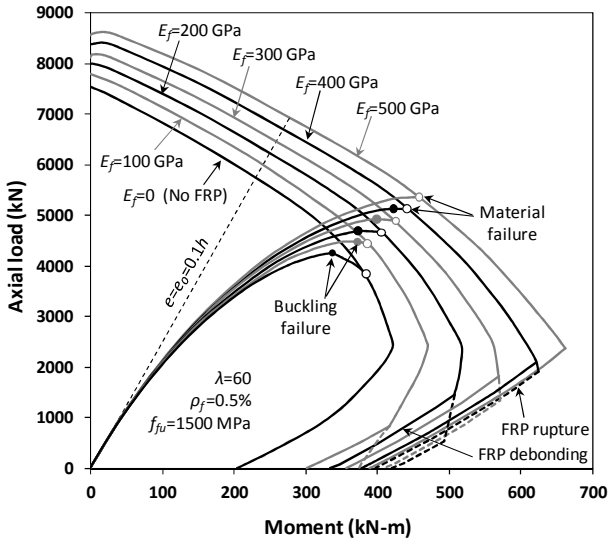

Fig. 13 Performance of RC columns of various CFRP Young's moduli

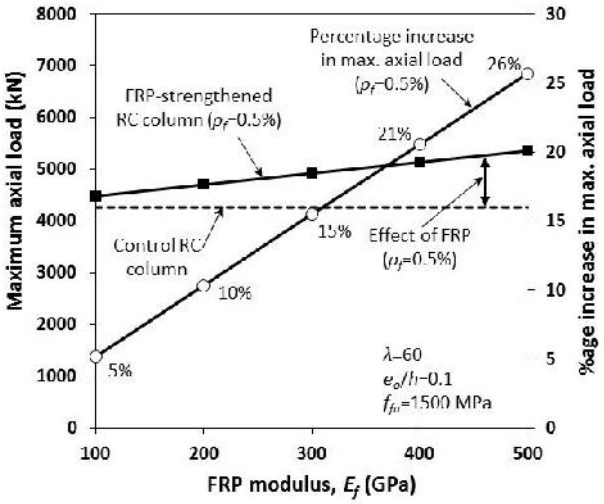

Fig. 14 Variation of strength gain due to CFRP retrofitting with CFRP Young's modulus

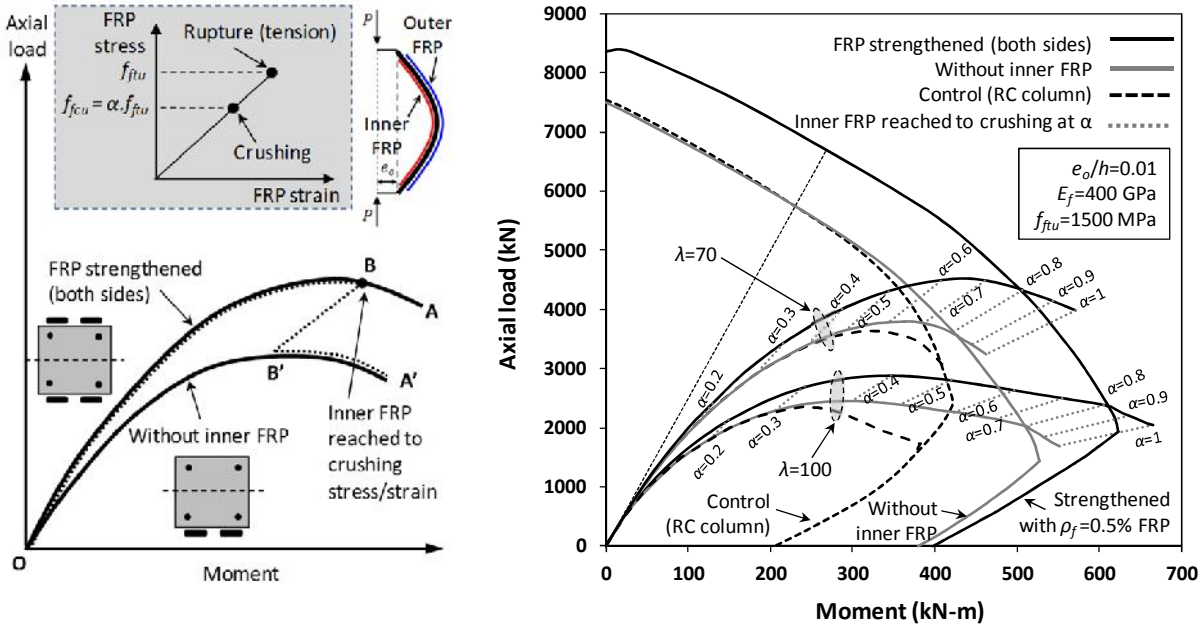

(a) Concept of FRP crushing and buckling **(b) Axial load-bending moment paths**

Fig. 15 Performance of RC columns of various CFRP crushing strength